Atmos. Chem. Phys. Discuss., https://doi.org/10.5194/acp-2017-813
Manuscript under review for journal Atmos. Chem. Phys.
Discussion started: 18 September 2017

Atmospheric Chemistry and Physics
Discussions

Characterizing biospheric carbon balance using CO_2 observations from the OCO-2 satellite

Scot M. Miller[1], Anna M. Michalak[1], Vineet Yadav[2], and Jovan M. Tadic[3]

[1]Department of Global Ecology, Carnegie Institution for Science, Stanford, CA, USA
[2]Jet Propulsion Laboratory, California Institute of Technology, Pasadena, CA, USA
[3]Lawrence Berkeley National Laboratory, Berkeley, CA, USA

Correspondence to: Scot M. Miller (scot.m.miller@gmail.com)

Abstract.

NASA's Orbiting Carbon Observatory–2 (OCO-2) satellite launched in summer of 2014. Its observations could allow scientists to constrain CO_2 fluxes across regions or continents that were previously difficult to monitor. This study explores an initial step toward that goal; we evaluate the extent to which current OCO-2 observations can detect patterns in biospheric CO_2 fluxes and constrain monthly CO_2 budgets. Our goal is to guide top-down, inverse modeling studies and identify areas for future improvement. We find that uncertainties and biases in the individual OCO-2 observations are comparable to the atmospheric signal from biospheric fluxes, particularly during northern hemisphere winter when biospheric fluxes are small. A series of top-down experiments indicate how these errors affect our ability to constrain monthly biospheric CO_2 budgets. We are able to constrain budgets for between two and four global regions using OCO-2 observations, depending on the month, and we can constrain CO_2 budgets at the regional level (i.e., smaller than seven global biomes) in only a handful of cases (16% of all regions and months). The potential of the OCO-2 observations, however, is greater than these results might imply. A set of synthetic data experiments suggests that observation or retrieval errors have a salient effect. Advances in retrieval algorithms and to a lesser extent atmospheric transport modeling will improve the results. In the interim, top-down studies that use current satellite observations are best-equipped to constrain the biospheric carbon balance across only continental or hemispheric regions.

1 Introduction

The OCO-2 satellite launched on July 2nd, 2014 and is NASA's first mission dedicated to observing CO_2 from space. The satellite measures the absorption of reflected sunlight within CO_2 and molecular oxygen (O_2) bands at near infrared wavelengths. These measurements are analyzed with remote sensing retrieval algorithms to yield spatially-resolved estimates of the column-averaged CO_2 dry air mole fraction, XCO_2. The satellite flies in a sun-synchronous orbit an average of 705 km above the Earth's surface, passing each location at approximately 13:30 local time, and it collects roughly 5×10^5 to 1×10^6 observations or soundings per calendar day (e.g., Crisp et al., 2004; Eldering et al., 2012; Crisp et al., 2017).

Unlike previous missions, OCO-2 observations are sensitive to CO_2 throughout the entire troposphere, advantageous for estimating surface CO_2 fluxes. By contrast, thermal infrared observations from existing meteorological sounders such as the

Atmospheric Infrared Sounder (AIRS), Tropospheric Emission Spectrometer (TES), and Infrared Atmospheric Sounding Interferometer (IASI) can yield estimates of the CO_2 concentration in the middle troposphere, but they have little sensitivity to near-surface CO_2 variations. Because OCO-2 observes in the near infrared, its observations are sensitive to CO_2 variations throughout the atmospheric column, with greatest sensitivity near the surface (e.g., Eldering et al., 2017).

A few studies comment on the possibilities of using XCO_2 observations for estimating CO_2 fluxes at the Earth's surface. For example, Chevallier et al. (2007) and Baker et al. (2010) explain that OCO-2 observations could reduce flux uncertainties by $\sim$20–65% at the the model grid scale (2.5° by 3.75° and 2° by 5° latitude-longitude, respectively) and at weekly time scales. Both studies, however, caution that biases or spatially and temporally correlated errors would cut this uncertainty reduction in half. Chevallier et al. (2007) further explain that biases of a few tenths of a part per million in XCO_2 could bias estimated subcontinental flux totals by several tenths of a gigaton.

Relatively few studies in the published literature use XCO_2 observations from OCO-2 to estimate fluxes, primarily due to the relatively short time since the satellite's launch (e.g., Fischer et al., 2017; Heymann et al., 2017). This paucity of studies will undoubtedly change in the next several years. The literature on other CO_2 remote sensing efforts is more mature, and these studies preview the opportunities and challenge that OCO-2 may present. For example, the Greenhouse Gas Observing Satellite (GOSAT) launched in 2009 and is the first satellite dedicated to greenhouse gas monitoring (Yokota et al., 2009). A number of studies use GOSAT observations to estimate surface fluxes, and these studies report numerous successes and challenges that could apply to OCO-2 (e.g., Takagi et al., 2011; Basu et al., 2013; Guerlet et al., 2013; Maksyutov et al., 2013; Parazoo et al., 2013; Saeki et al., 2013; Basu et al., 2014; Deng et al., 2014; Houweling et al., 2015). GOSAT observations provide new insight into fluxes in regions that are poorly sampled by in situ observations, regions like tropical Asia (Basu et al., 2014) and the southern Amazon (Parazoo et al., 2013). These studies also identify a number of common challenges. For example, observations are too sparse to reliably estimate fluxes in regions with frequent cloud cover (e.g., Parazoo et al., 2013). Furthermore, continental CO_2 budgets estimated using GOSAT observations are not consistent with in situ observations in some regions; these differences may indicate spatially and temporally correlated errors in GOSAT observations at their current stage of development (e.g., Houweling et al., 2015). These challenges are also a concern for OCO-2. With that said, some design features make OCO-2 even more promising than GOSAT: OCO-2 observations have a higher spatial resolution (e.g., a footprint or pixel size of about 3 km^2 relative to GOSAT's footprint of about 80 km^2) and a higher density of observations (e.g. Crisp et al., 2004; National Research Council, 2010).

This study evaluates the opportunities and challenges of using current OCO-2 observations to estimate biospheric CO_2 fluxes. A primary goal of this work is to guide top down, inverse modeling studies on the information content of currently-available observations. By contrast, satellite capabilities for CO_2 monitoring will likely change quickly over the next ten years – both due to improvements in satellite retrieval algorithms and the launch of new satellites (Sect. 4). This guidance will therefore undoubtedly change and evolve in the future.

We evaluate current OCO-2 observations using several approaches. We make an initial assessment by comparing model and observation errors against the atmospheric signal from biospheric fluxes. The noise in individual observations is important, but atmospheric inversions ultimately leverage broad patterns in the observations and other complex information to estimate

Atmos. Chem. Phys. Discuss., https://doi.org/10.5194/acp-2017-813
Manuscript under review for journal Atmos. Chem. Phys.
Discussion started: 18 September 2017

surface fluxes. We therefore construct a series of top-down simulations using OCO-2 observations to understand what these errors mean for estimating CO_2 fluxes, and we thereby evaluate the number of global regions for which we can independently constrain CO_2 budgets. Lastly, we construct a series of synthetic data simulations to diagnose the real data results. The first synthetic simulations do not include any errors – to evaluate the inherent strengths of the observations. In subsequent synthetic simulations, we include simulated modeling and/or retrieval errors, and evaluate how these errors affect the CO_2 flux constraint.

The synthetic and real data simulations are based upon a multiple regression combined with model selection. We use this approach to evaluate whether spatial and temporal patterns in biospheric CO_2 fluxes help describe patterns in the OCO-2 observations. These flux patterns are first input into a global atmospheric transport model (the Parameterized Chemistry Transport Model or PCTM, Kawa et al., 2004) and are then compared against OCO-2 observations. A positive result implies that we can detect these patterns using OCO-2 observations, and a negative result implies that we cannot. Several existing studies use model selection to gauge the detectability of CO_2 flux patterns (Shiga et al., 2014; Fang et al., 2014; ASCENDS Ad Hoc Science Definition Team, 2015). The term 'patterns' here refers to flux patterns that manifest at the resolution of an atmospheric model, and section 2 describes this approach in more detail.

Overall, we divide the globe into different hemispheres and biomes and determine whether we can detect flux patterns within each region and each month. We begin the analysis with very large hemispheric regions and then decrease the size of those regions until we are no longer able to detect any patterns beyond a mean CO_2 flux. That limit or end point is the smallest scale at which OCO-2 observations currently provide a unique constraint on CO_2 budgets. OCO-2 observations must be sufficient to detect more than a mean flux across a region and month if future inverse modeling studies are to estimate biospheric CO_2 budgets at scales smaller than that region. Consequently, inverse modeling studies would generally be unable to obtain reliable information about the fluxes across smaller regions. This result bounds the type of information one can expect from the OCO-2 retrievals in their current stage of development.

2 Methods

2.1 Simulated model and retrieval errors

We simulate different model and measurement errors and compare those errors against a modeled XCO_2 signal from biospheric fluxes. This section describes the simulated errors – both simulated atmospheric transport and observation or retrieval errors (Fig. 1). The SI describes these errors in greater detail.

We use estimated CO_2 transport errors from Liu et al. (2011) and Miller et al. (2015) (Fig. 1a–b). The authors of those studies run an ensemble of global meteorology simulations. CO_2 is included as a passive tracer in the model, and all simulations use the same CO_2 flux estimate but have different meteorology. The authors estimate CO_2 transport errors by examining the range of CO_2 mixing ratios in the ensemble of simulations. We choose one realization at random and subtract the mean of the ensemble from this realization to produce a set of residuals. These residuals are used as the estimated transport errors in this study. The estimated errors are therefore a realization of plausible transport errors. As a result, the specific errors used here have the same statistical properties as the other members of the ensemble but have different values in specific locations or at

Atmos. Chem. Phys. Discuss., https://doi.org/10.5194/acp-2017-813
Manuscript under review for journal Atmos. Chem. Phys.
Discussion started: 18 September 2017

Atmospheric Chemistry and Physics
Discussions

specific times. For example, the transport errors have a negative value across much of the Arctic in Fig. 1a. Other ensemble members, by contrast, might have a slight positive bias in that region but will nevertheless have similar statistical properties as the realization in Fig. 1a.

In addition to these transport errors, we simulate observation or retrieval errors. We use two different approaches to estimate these errors and report results using both approaches. The true retrieval errors are unknown and any effort to estimate these errors will be uncertain; the two approaches used here provide two contrasting, plausible representations of these errors.

We generate the first set of possible retrieval errors using the parameters used to correct OCO-2 retrievals. This approach entails several steps. We first try to reproduce the OCO-2 observations using a regression. The predictor variables in this regression include seven different terrestrial biosphere model (TBM) estimates of net biome production and vegetation indices that have been input into an atmospheric transport model. We also include anthropogenic, ocean, and biomass burning flux estimates in the regression. A subsequent section (Sect. 2.2) describes this regression in greater detail. We save the model-data residuals from this regression. Subsequently, we regress these residuals on the parameters used in the OCO-2 bias correction. These include aerosol optical depth and albedo, among other parameters (e.g., Wunch et al., 2011, see Sect. S1.4). Note that these retrieval parameters are not run through an atmospheric transport model, unlike the TBMs and vegetation indices. We estimate the observation or retrieval errors as the portion of the model-observation residuals that are described by these retrieval parameters. The regression considers many different TBMs and vegetation indices, and it should therefore do reasonably well at reproducing patterns in the OCO-2 observations attributable to biospheric fluxes. Any remaining patterns in the data that map on to retrieval parameters are likely due to retrieval errors rather than transport or flux errors.

We use a second approach to create an alternative set of simulated retrieval errors. We model XCO_2 using four alternative biospheric flux estimates (Sect. 2.2) and compute the model-data residuals for each set of simulations. We identify the grid cells in which all four sets of residuals have the same sign (i.e., generated using four different flux estimates) and identify all of the model grid cells in which the residuals have variable sign. In the former case, we take the median of all four residuals as the estimated retrieval error and, in the latter case, assign a retrieval error of zero.

2.2 Model selection overview

Model selection is a statistical approach common in regression modeling (e.g., Ramsey and Schafer, 2012, ch. 12). In many instances, a modeler must decide which predictor variables to include (or omit) in a multiple regression. Model selection will identify the set of variables with the greatest power to describe the data. It also ensures that the regression does not overfit the data. The inclusion of more predictor variables in a regression will always improve model-data fit; a regression with n independent predictor variables will always be able to describe n data points perfectly. However, a model with n independent predictor variables would overfit the data (for more on the dangers of overfitting, refer to Zucchini, 2000). To this end, one can use model selection to prevent overfitting and only include predictor variables that describe substantial variability in the data.

A number of existing top-down studies of CO_2 use model selection (e.g., Gourdji et al., 2008, 2012; Shiga et al., 2014; Fang et al., 2014; Fang and Michalak, 2015; ASCENDS Ad Hoc Science Definition Team, 2015). Several use the approach to determine a set of environmental variables to include in a geostatistical inverse model (e.g., Gourdji et al., 2008, 2012). Other

Atmos. Chem. Phys. Discuss., https://doi.org/10.5194/acp-2017-813
Manuscript under review for journal Atmos. Chem. Phys.
Discussion started: 18 September 2017

Atmospheric Chemistry and Physics
Open Access
Discussions

studies use model selection to determine whether existing CO_2 observations can constrain flux patterns from the biosphere (Fang et al., 2014) and from fossil fuel emissions (Shiga et al., 2014; ASCENDS Ad Hoc Science Definition Team, 2015). One study uses model selection to assess the capabilities of a proposed satellite mission (ASCENDS Ad Hoc Science Definition Team, 2015).

We use model selection to explore whether current OCO-2 observations are sufficient to detect broad spatial and temporal patterns in CO_2 fluxes – within two large hemispheric regions, four continental regions, and seven biomes (Fig. 2). The last goal is more challenging than the first. In each case, we use model selection to examine whether the flux patterns within each region and each month help reproduce patterns in the OCO-2 observations.

We begin with a baseline model that has spatial and temporally constant fluxes for each region and month of interest. These constant terms are analogous to the intercept in a multiple regression. These intercept terms are always included (e.g., Gourdji et al., 2008; Fang et al., 2014), and we use model selection to identify additional model outputs as necessary.

We subsequently model XCO_2 using an atmospheric transport model (Sect. 2.4) and several different biospheric flux estimates and vegetation indices. We then incorporate these model outputs as predictor variables in a regression and use model selection to identify which patterns (if any) explain substantial variability in the OCO-2 observations. These patterns include four TBMs with contrasting spatial features from MsTMIP, the Multi-scale Synthesis and Terrestrial Model Intercomparison Project (Huntzinger et al., 2013; Fisher et al., 2016a, b). Section S1.2 describes MsTMIP and the TBMs in greater detail. We also include SIF (solar-induced fluorescence) from the Global Ozone Monitoring Experiment-2 (GOME-2, Joiner et al., 2013) as well as EVI (enhanced vegetation index) and NDVI (normalized difference vegetation index) from the Moderate-Resolution Imaging Spectroradiometer (MODIS; e.g., Huete et al., 2002). Note that we directly input these vegetation indices into an atmospheric transport model as a surface 'flux.' The regression/model selection framework will adjust the magnitude of the transport model outputs to reproduce the OCO-2 observations, so the absolute magnitude of the vegetation indices is not important. Rather, we are interested in whether the patterns in these vegetation indices help reproduce patterns in the OCO-2 observations, potentially in combination with other indices or TBMs.

We offer up a relatively large number of flux models and vegetation indices as predictor variables, and at least some of these products are therefore expected to correlate with real world CO_2 fluxes. We should choose at least one of these variables using model selection if the OCO-2 observations are able to detect patterns in the surface fluxes. If we do not choose any additional outputs with model selection, it suggests that the observations are not sufficient to detect spatial and temporal patterns in the fluxes beyond a mean flux. We include a large number of candidate variables for a pragmatic reason. If model selection does not pick any variable in a region, it is unlikely that there was a shortage of reasonable CO_2 flux patterns available to choose from. Rather, that result more likely reflects the maturity of current OCO-2 observations and atmospheric modeling capabilities.

Model selection provides a convenient way to evaluate the information content of OCO-2 observations in their current state of development. In theory, one could estimate CO_2 budgets in a Bayesian inverse model. The accuracy or uncertainty in those budgets would be indicative of the information content of the satellite observations. This approach, however, brings several challenges. First, a modeler must choose a prior flux estimate. This choice is often subjective but will impact the final or posterior uncertainty estimate (e.g., Chevallier et al., 2014). Second, a modeler must estimate several individual sources of

Atmos. Chem. Phys. Discuss., https://doi.org/10.5194/acp-2017-813
Manuscript under review for journal Atmos. Chem. Phys.
Discussion started: 18 September 2017

uncertainty as inputs to the inverse model. These uncertainties often have a complex statistical structure that is difficult to characterize (e.g., Liu et al., 2011), and it is often challenging to account for all plausible sources of uncertainty. Third, inverse modeling with satellite observations can be computationally intensive – both in terms of the number of atmospheric model simulations required and the computational requirements of the statistical inverse model. Some studies have overcome the first of these two challenges by using an ensemble of atmospheric models and/or inversion systems (e.g., Chevallier et al., 2014; Houweling et al., 2015). The size of the ensemble spread is indicative of the information content of the observations, and the spread of the ensemble is usually larger than the uncertainty bounds estimated from any one inverse model. This type of study also typically requires extensive coordination among multiple research groups. Model selection, by contrast, provides a simpler metric to evaluate the information content of the observations.

The remainder of this sub-section describes the specific equations used for model selection. We quantitatively link the OCO-2 XCO_2 observations with model outputs using a multiple regression:

$$\mathbf{Y} = h(\mathbf{X}) \tag{1}$$

$$\boldsymbol{z} = \mathbf{Y}\boldsymbol{\beta} + \boldsymbol{\epsilon} \tag{2}$$

$$\boldsymbol{\epsilon} \sim \mathcal{N}(\mathbf{0}, \sigma^2\mathbf{V}) \tag{3}$$

In these equations, the vector $\boldsymbol{z}$ (dimensions $n \times 1$) represents the XCO_2 observations minus the model initial condition or spin-up (refer to the SI for more detail). The variable $\mathbf{X}$ (dimensions $m \times p$) is a matrix of p different flux patterns; the columns of $\mathbf{X}$ can include biospheric CO_2 flux estimates, remote sensing vegetation indices, an anthropogenic emissions inventory, a biomass burning inventory, and/or an ocean flux estimate. The function $h()$ is an atmospheric model that transports the fluxes to the times and locations of the OCO-2 retrievals, and the resulting matrix $\mathbf{Y}$ has dimensions $n \times p$. The variable $\boldsymbol{\epsilon}$ is a $n \times 1$ vector of residuals. These residuals are assumed to follow a multivariate normal distribution with a mean of zero, a variance of σ^2, and a covariance structure given by $\mathbf{V}$ (dimensions $n \times n$). The vector of coefficients ($\boldsymbol{\beta}$, dimensions $p \times 1$) are estimated as part of the regression.

In this study, we choose a set of variables for $\mathbf{X}$ using model selection based on the Bayesian Information Criterion (BIC) (Schwarz, 1978). We calculate a BIC score for many different candidate models. Each candidate model has a different set of columns ($\mathbf{X}$) – different combinations of flux models or remote sensing vegetation indices in different geographic regions and in different months.

The best model has the lowest BIC score:

$$BIC = L + p\ln(n^*) \tag{4}$$

where L is the log likelihood of a particular candidate model ($\mathbf{X}$). The log likelihood equation rewards models that improve model-data fit, and the second term in the equation ($p\ln n^*$) penalizes complex models; it ensures that the selected model is not an over-fit. The log-likelihood has the following form:

$$L = n^* \ln(\sigma^2) + \frac{n^*}{n} RSS \quad (5)$$

$$RSS = \frac{1}{\sigma^2}\boldsymbol{z}^T\boldsymbol{z} - \frac{1}{\sigma^2}\boldsymbol{z}^T\mathbf{Y}(\mathbf{Y}^T\mathbf{Y})^{-1}\mathbf{Y}^T\boldsymbol{z} \quad (6)$$

where RSS is the residual sum of squares and σ^2 is defined above in Eq. 3.

Both the BIC and log-likelihood equations (Eq. 4 and 6) incorporate n^*, the effective number of independent observations. Jones (2011) discusses this concept in the context of the BIC. Just because the satellite provides n observations does not mean there are n independent pieces of information. Accordingly, n^* ensures that the model selection framework accurately assesses the amount of independent information in the observations. It accounts for the fact that there are often spatial and temporally coherent errors in the satellite observations or in the transport model. If all of the observations were independent (i.e., if $\mathbf{V}$ were diagonal), then n^* would equal n. However, we de-weight both components of Eq. 4 as the covariances in $\mathbf{V}$ increase.

We could calculate n^* directly using $\mathbf{V}^{-1}$ (Jones, 2011). In fact, several CO_2 model selection studies incorporate $\mathbf{V}^{-1}$ directly into the equation for RSS (e.g., Mueller et al., 2010; Gourdji et al., 2012; Shiga et al., 2014). We use 5,079,165 observations (n) in this study, so $\mathbf{V}$ has 5.08×10^6 rows and columns. As a result, the inverse of $\mathbf{V}$ is computationally intractable. We instead estimate n^* using an approach based on Griffith (2005), an approach that does not require computing $\mathbf{V}^{-1}$ directly:

$$n^* = \frac{n}{1 + \left(\sum_{i=1}^{n}\sum_{j=1, j\neq i}^{n} V_{i,j}/n\right)} \quad (7)$$

We estimate $V_{i,j}$ in the vicinity of each observation i by fitting a local variogram model on the model-data residuals (ϵ) (See Alkhaled et al. (2008) and Hammerling et al. (2012) for a description of local variogram analysis.). The SI describes this implementation in greater detail.

2.3 OCO-2 data

This study utilizes XCO_2 observations from the OCO-2 satellite beginning with the first reported data (6 Sept. 2014) through the end of 2015. We use the level 2 lite product, version B7.1.01; the lite product only includes good quality retrievals, unlike the full OCO-2 level 2 product. We only include nadir and target mode retrievals in the analysis and exclude glint mode retrievals. Recent work indicates biases in the glint retrievals relative to nadir retrievals (e.g., Wunch et al., 2017). The SI describes model selection results with glint mode retrievals included, and the results are similar to those in the main manuscript without glint mode data.

2.4 Atmospheric transport model

We employ PCTM to model XCO_2 using a variety of surface flux estimates and vegetation indices (Kawa et al., 2004). A number of existing studies use this model to simulate atmospheric CO_2 mixing ratios (e.g., Law et al., 2008; Gurney et al., 2009; Baker et al., 2010; Schuh et al., 2010; Shiga et al., 2013; ASCENDS Ad Hoc Science Definition Team, 2015; Hammerling

Atmos. Chem. Phys. Discuss., https://doi.org/10.5194/acp-2017-813
Manuscript under review for journal Atmos. Chem. Phys.
Discussion started: 18 September 2017

et al., 2015). Several of these studies specifically use PCTM to model CO_2 in the context of satellite missions (e.g., Baker et al., 2010; ASCENDS Ad Hoc Science Definition Team, 2015; Hammerling et al., 2015). The PCTM configuration in this study has global coverage, a spatial resolution of 1° latitude by 1.25° longitude, and 56 vertical levels. We both input the fluxes and estimate atmospheric mixing ratios at a 3-hourly time resolution, and the model transports fluxes through the atmosphere using winds from NASA's Modern-Era Retrospective Analysis for Research and Applications (MERRA) (Rienecker et al., 2011). Section S1.1 includes more detail on the model initial condition and spin-up period.

2.5 Real and synthetic data simulations

We initially use real observations to examine whether current OCO-2 observations can detect biospheric flux patterns in each month and each region of the globe. We consider the model selection results from 2014 part of an initial model spin-up period and only report the results from 2015.

We also consider non-biospheric fluxes for use in $\mathbf{X}$. We include anthropogenic emissions from EDGAR v4.2 FT2010 (European Commission, Joint Research Centre (JRC)/Netherlands Environmental Assessment Agency (PBL), 2013; Olivier et al., 2014), climatological ocean fluxes from Takahashi et al. (2016), and biomass burning fluxes from the Global Fire Emissions Database (GFED), version 4.1 (van der Werf et al., 2010; Giglio et al., 2013). We are not interested in anthropogenic or marine fluxes per se. Rather, we want to account for these fluxes in the modeling framework and do not want any omissions to affect inferences related to biospheric fluxes. As a result, we do not separate these non-biospheric fluxes by region or month because these sources are not the focus of this study; each of these sources is assigned a single column in $\mathbf{X}$. Furthermore, we do not include these variables by default within $\mathbf{X}$, unlike the constant flux base model. Rather, they are included as candidate variables within the model selection framework.

In the seven region case, $\mathbf{X}$ has a minimum of 112 columns and a maximum of 899 columns – 112 columns associated with the constant flux base model, 784 columns associated with biospheric flux patterns, and three columns associated with fossil fuel, ocean, and biomass burning fluxes.

We further utilize synthetic data simulations in this study to evaluate the potential of OCO-2 observations and analyze the effects of different model or retrieval/observation errors. In these simulations, we create synthetic XCO_2 observations using PCTM and the SiBCASA model. We then run model selection using these synthetic data. These model selection runs have the same setup as the real data simulations, except that the observations (z) are synthetic instead of real. Furthermore, we only analyze the seven region case in the synthetic data experiments. This case is more stringent than the two and four region cases. The seven biome case is also an important goal from a ecological perspective: one might want to estimate how CO_2 fluxes differ in different tropical forests or in different temperate forests (e.g., on different continents or in different climate zones). The in-situ monitoring network in North America, for example, is able to detect flux patterns within most North American biomes (Fang et al., 2014), and this standard of detectability would be a rigorous goal for satellites to achieve.

The first model selection runs are an idealized case with no simulated errors ($\boldsymbol{\epsilon} \approx \mathbf{0}$). We then successively add simulated error to the synthetic observations and evaluate how the model selection results change as the errors increase (Fig. 1). We include three different types of errors: flux errors, transport errors, and observation or retrieval errors. Section 2.1 and the SI

Atmos. Chem. Phys. Discuss., https://doi.org/10.5194/acp-2017-813
Manuscript under review for journal Atmos. Chem. Phys.
Discussion started: 18 September 2017

describe the simulated transport and retrieval errors. The flux errors further account for plausible inaccuracies in the predictor variables within $\mathbf{X}$. No TBM or vegetation index has a distribution that perfectly matches real-world CO_2 fluxes. These errors affect our ability to identify biospheric flux patterns using the OCO-2 observations and would affect inverse modeling studies; the better the prior flux estimate in an inverse model, the more accurate and reliable the posterior flux estimate. We therefore account for these flux errors in the synthetic data simulations. To this end, we remove SiBCASA as an option in the $\mathbf{X}$ matrix and choose among the other remaining patterns. This procedure simulates the plausible effects of imperfect TBMs or predictor variables.

3 Results & discussion

3.1 The biospheric CO_2 signal versus model and measurement noise

We compare simulated model and measurement errors against the atmospheric signal from biospheric fluxes (Fig. 3). The comparison provides an intuition of the 'noise' and the CO_2 'signal' given current modeling and observation capabilities. This atmospheric CO_2 signal from biospheric fluxes is marked, even when averaged across a total vertical column. Globally, the XCO_2 signal has a mean absolute value of 0.5ppm in February and 1.3ppm in July. The 10th and 90th percentiles are 0.04 and 1.4ppm in February and 0.06 and 3.8ppm in July. In July, the largest enhancements are in the northern hemisphere mid and high latitudes while the largest enhancements during winter months are in the tropics and southern hemisphere.

The simulated model and retrieval/observation errors are comparable to this XCO_2 signal from biospheric fluxes. These errors have a mean absolute value of 0.6ppm in both February and July. The 10th and 90th percentiles are 0.08 and 1.35ppm in February and 0.08 to 1.25ppm in July. Using the alternative retrieval estimate, the errors and percentiles are 0.8, 0.02, and 2.1ppm in February and 1.4, 0.05, and 3.7ppm in July. Phrased differently, these errors, averaged across all nadir and target data, equate to 115 – 122% of the mean biospheric CO_2 signal in February and 43 – 107% in July, depending upon the retrieval error estimate. Figure 3 further indicates the spatial distribution of the atmospheric CO_2 'signal' and 'noise.' It is important to note that the total number of OCO-2 observations is large (e.g., 268,671 and 343,053 nadir and target observations in February and July, respectively, in the lite data file), but the distribution of these observations is heterogeneous across the globe. For example, the data are concentrated in tropical and temperate regions and are sparse at high latitudes and regions with frequent cloud cover (e.g., the Amazon).

The relative magnitude of the errors provides an informative measure of the observations, but it does not tell the complete story. A number of other considerations affect scientists' ability to estimate surface fluxes using these observations. First, inverse models leverage more than the point-wise signal to estimate surface fluxes; these models leverage complex spatial and temporal patterns in the data to estimate surface fluxes. Second, the absolute magnitude or variance of the errors is only one consideration. Another important factor is the spatial and temporal correlations or covariances in these errors. These covariances reduce the independent information in the data and can obscure patterns in XCO_2 that are due to surface fluxes. As a result, we construct real and synthetic data experiments to understand what these errors mean for estimating surface fluxes.

Atmos. Chem. Phys. Discuss., https://doi.org/10.5194/acp-2017-813
Manuscript under review for journal Atmos. Chem. Phys.
Discussion started: 18 September 2017

3.2 Real data experiments

The model selection experiments using real data indicate the number or size of regions for which we can reliably constrain biospheric CO_2 budgets using current OCO-2 observations. We start the real data simulations with large hemispheric regions and reduce the size of the regions until we are no longer able to detect any CO_2 flux patterns or information beyond a mean monthly flux in each region and each month. We would need to detect more than a mean flux from a given region if we are to reliably constrain fluxes across smaller regions.

The first real data experiment indicates whether the observations are sufficient to detect flux patterns within two large hemispheric regions (Fig. 2). Figure 4a displays the number of months in which at least one pattern is chosen, broken down by region. The results in Fig. 4a are grouped by season for convenience. Dark colors suggest excellent detectability for a given region and season while light colors suggest limited detection abilities.

Model selection identifies flux patterns in about half of all months. This outcome suggests that OCO-2 and the PCTM model can be used to identify broad, hemispheric flux patterns. One important exception is the extra-tropics (e.g., the temperate, boreal, and arctic region), in both spring and fall. Biospheric uptake in these seasons is less than the summer maximum, in both the northern and southern hemispheres. As a result, flux patterns in these areas are not as heterogeneous and not readily detectable using the satellite observations. This result also indicates that the OCO-2 observations can be used to reliably constrain CO_2 budgets at scales smaller than hemispheric in about half of all cases.

In a second experiment, we try to identify flux patterns within four, smaller regions using OCO-2 observations and model selection (Fig. 4b). We choose flux patterns in 29% of all regions and months using model selection. This experiment is more demanding than the first, and it is therefore unsurprising that we choose fewer flux patterns; flux patterns within these four continental regions are often less heterogeneous than across the two large hemispheric regions in the first experiment. This result suggests that inverse modeling studies would be able to constrain CO_2 budgets at more detailed spatial scales in about one third of all regions and months.

The third and final experiment includes seven biomes, and we choose relatively few flux patterns using model selection in this final experiment (16% of all possible regions and months, Fig. 4c). This result suggests a limited ability to detect biospheric flux patterns within each of the seven global biomes. Inverse modeling studies would thus be able to uniquely constrain CO_2 budgets across smaller regions in only a small handful of cases (e.g., 16% of all possible regions and months). These results appear similar to a recent study using current GOSAT retrievals. Houweling et al. (2015) compare an ensemble of inverse modeling flux estimate using GOSAT. Estimates show good agreement across very large regions (e.g., within 20% for global, annual CO_2 budgets) but disagree by over 100% over subcontinental-sized TransCom regions (e.g., Gurney et al., 2002).

As part of model selection, we also estimate the effective number of independent OCO-2 observations, referred to as n^* (Eq. 7). Correlations or covariances in transport and retrieval errors will reduce the value of n^*. Our estimate is similar among all of the real data experiments and is approximately 4000 (4060 for the two region case, 3600 for the four region case, and 3540 for the seven region case). By comparison, the total number of OCO-2 observations during the study period (n) is 5.08×10^6. This ratio corresponds to one independent observation per $\sim$1200 OCO-2 lite retrievals.

3.3 Synthetic data experiments

The goal of the synthetic data simulations is to understand the challenges that influence the real data results. If future efforts can mitigate these challenges, then inverse modeling studies would be able to reliably constrain flux patterns and CO_2 budgets across individual biomes or even smaller regions.

We first construct an idealized synthetic data study without any errors (Fig. 5a), and we choose a flux pattern for every biome in every month using model selection. This case study indicates that the OCO-2 observations are not insensitive to biospheric fluxes at the surface. This result is not necessarily an obvious one. Some satellite instruments, particularly those that measure in the thermal infrared, are most sensitive to mixing ratios in the upper troposphere and have limited sensitivity to the surface (e.g., AIRS, see Chevallier et al., 2005). OCO-2, by contrast, observes in the shortwave infrared and is sensitive to CO_2 mixing ratios throughout the troposphere.

Subsequent model selection experiments include at least one error type, and these results all look different from the first, idealized case. We choose patterns in fewer regions and months with model selection when we include one error type (Fig. 5b-d). Of the three different error types, observation or retrieval errors have the largest impact on the model selection results (Fig. 5d). Note that the retrieval errors used to generate Fig. 5d are those simulated in Fig. 1c-d. Section S2.2 describes the model selection experiments using an alternative set of retrieval errors (Fig. 1e-f), and these results are similar to those presented in the main manuscript (Fig. 5).

Notably, the addition of any error, large or small, appears to hinder flux pattern detection in marginal biomes – biomes with small fluxes and/or small spatial and temporal variability (e.g., tundra and deserts). Arguably, this result is unsurprising. OCO-2 observations are sparse in many cloudy, high latitude regions, and CO_2 fluxes are weak at high latitudes and in deserts. Fluxes from these regions are quickly obscured by even modest errors in the model or observations. Future CO_2 remote sensing efforts would have difficulty detecting biospheric patterns within these areas. Other regions, like forests and grasslands, have larger and/or more heterogeneous fluxes, and these patterns should be easier to detect with satellite observations.

The experiments in Fig. 5e-g include two different error types, and we choose fewer months and regions with model selection relative to the previous cases. The experiment with transport and flux errors (but not retrieval errors, Fig. 5e) still show good detectability during the summer months and in temperate and tropical forest and grassland biomes. By contrast, the experiments that include retrieval errors (Fig. 5f-g) show limited detectability in all biomes and seasons.

The last experiment (Fig. 5h) includes all error types. We obtain positive results in fewer regions in fewer months relative to other cases. These results are broadly consistent with the real data experiments; we choose a similar number of regions and seasons in both this experiment and the real data experiment (Fig. 5h). This consistency indicates that the synthetic simulations likely mirror real-world conditions. Note that the estimate for n^* in this final synthetic experiment is about half that of n^* in the real data experiments ($n^* = 1630$). These synthetic experiments may therefore slightly overestimate the spatial and temporal covariance of the errors relative to real data.

Overall, the synthetic simulations suggest that observation or retrieval errors play a salient role relative to other error types (e.g., transport errors or flux errors, Fig. 5). Spatial and temporal error covariances and biases may be at least partly to blame.

The estimated transport errors are spatially and temporally correlated on synoptic time scales (e.g., Miller et al., 2015). These scales are generally smaller than the biomes and hemispheres examined in this study. As a result, these errors will average down over time and space, and this averaging will mitigate the impact of these errors on the results. This statement, of course, only holds if there are no large-scale biases in the meteorology. The simulated observation or retrieval errors, by comparison, covary across longer spatial and temporal scales. These errors correlate with retrieval parameters like aerosol optical depth or albedo that often change at broader seasonal or regional scales. The greater these error correlations, the less these errors average down across space and time, and the greater impact these errors have on the utility of XCO_2 observations. A reduction in the spatial and temporal coherence of these errors would improve the model selection results.

4 Conclusions

The OCO-2 satellite offers a new, global window into atmospheric CO_2 and CO_2 fluxes at the Earth's surface. This study explores a first step in realizing these capabilities; we evaluate the extent to which current OCO-2 observations can detect patterns in biospheric CO_2 fluxes and constrain monthly CO_2 budgets.

We find that OCO-2 observations, in their current state of development, often provide a reliable constraint on CO_2 budgets across continental or hemispheric regions. By contrast, we find that current observations can provide a unique CO_2 estimate across smaller regions in only a handful of cases. As a result, inverse modeling studies are unlikely to constrain regional fluxes at fine spatial and temporal scales given the current maturity of the observations. Regional CO_2 budgets estimated using these observations would be highly uncertain and prone to biases.

These results do not reflect any inherent limitation in the sensitivity of the OCO-2 satellite. Rather, they are likely the product of observation or retrieval errors and to a lesser extent atmospheric transport errors. Hence, the value or potential of the OCO-2 observations is greater than these results might otherwise imply. For example, our simulated retrieval errors often covary across large regions and across a month or more. Future improvements to retrieval algorithms could reduce both the variance and covariance of these errors, enabling confident CO_2 flux constraints across smaller regions.

Even with these limitations, current OCO-2 observations provide new information on CO_2 fluxes for many regions of the globe. On one hand, in situ data appear to provide a stronger constraint on CO_2 fluxes in some well-instrumented regions of the world, like North America (e.g., Fang et al., 2014). Our results using OCO-2 and seven global biomes are less successful. On the other hand, in situ observations are sparse in many regions of the world, including in most of the tropics, Africa, South America, and Asia (e.g., NOAA Global Monitoring Division, 2017). Current OCO-2 observations bring new monitoring capabilities to these regions that are unlikely to be matched by in situ observations within the near future.

Furthermore, a number of new satellite missions will launch in the next five years. Multiple sets of observations, in tandem, will provide a more detailed, robust constraint on CO_2 fluxes. For example, the GOSAT-2 satellite will monitor atmospheric CO_2 with better accuracy relative to the original GOSAT satellite (Japan Aerospace Exploration Agency, 2017). This improvement in both the quality and overall quantity of CO_2 observations will enable more detailed estimates of CO_2 fluxes. In addition to GOSAT-2, the OCO-3 mission will observe CO_2 from the International Space Station at a different locations and times of day relative to OCO-2 (NASA Jet Propulsion Laboratory, 2017). This feature will provide a stronger constraint on spatial and temporal variations in CO_2 fluxes. In addition, observation or retrieval errors appear to be a key factor in our results and will likely be a challenge for these future missions. Work on the OCO-2 retrieval algorithm will inform these upcoming missions, so improvements to the OCO-2 retrievals will likely improve the data capabilities of future missions as well. Further improvements to the satellite retrieval and atmospheric transport modeling could enable OCO-2 and future missions to provide detailed CO_2 budgets for much finer regions.

Competing interests. The authors declare that they have no conflict of interest.

Acknowledgements. We thank David Baker, David Crisp, Benjamin Poulter, and Eva Sinha for their help and feedback on the manuscript. The OCO-2 data are produced by the OCO-2 project at the Jet Propulsion Laboratory, California Institute of Technology, and obtained from the OCO-2 data archive maintained at the NASA Goddard Earth Science Data and Information Services Center. OCO-2 data are publicly available online at https://co2.jpl.nasa.gov/#mission=OCO-2. The MODIS EVI and NDVI data products are available online at https://lpdaac.usgs.gov/ courtesy of the NASA Land Processes Distributed Active Archive Center (LP DAAC), USGS/Earth Resources Observation and Science (EROS) Center, Sioux Falls, South Dakota. GOME-2 SIF data are available at https://acd-ext.gsfc.nasa.gov/People/Joiner/my_gifs/GOME_F/GOME-F.htm courtesy of Joanna Joiner. MsTMIP data products are archived at the ORNL DAAC (http://daac.ornl.gov), and 3-hourly flux products are available at dx.doi.org/10.3334/ORNLDAAC/1315. This work is funded by the Carnegie Distinguished Post-doctoral Fellowship and NASA grant #NNX13AC48G. Funding for MsTMIP was provided through NASA ROSES Grant #NNX10AG01A. Data management support for preparing, documenting, and distributing model driver and output data was performed by the Modeling and Synthesis Thematic Data Center at Oak Ridge National Laboratory (ORNL; http://nacp.ornl.gov), with funding through NASA ROSES Grant #NNH10AN681.

References

Alkhaled, A. A., Michalak, A. M., Kawa, S. R., Olsen, S. C., and Wang, J.-W.: A global evaluation of the regional spatial variability of column integrated CO_2 distributions, J. Geophys. Res.-Atmos., 113, doi:10.1029/2007JD009693, d20303, 2008.

ASCENDS Ad Hoc Science Definition Team: Active Sensing of CO_2 Emissions over Nights, Days, and Seasons (ASCENDS) Mission: Science Mission Definition Study, NASA, http://cce.nasa.gov/ascends_2015/ASCENDS_FinalDraft_4_27_15.pdf (last access: 30 Aug 2017), 2015.

Baker, D. F., Bösch, H., Doney, S. C., O'Brien, D., and Schimel, D. S.: Carbon source/sink information provided by column CO_2 measurements from the Orbiting Carbon Observatory, Atmos. Chem. Phys., 10, 4145–4165, doi:10.5194/acp-10-4145-2010, 2010.

Basu, S., Guerlet, S., Butz, A., Houweling, S., Hasekamp, O., Aben, I., Krummel, P., Steele, P., Langenfelds, R., Torn, M., Biraud, S., Stephens, B., Andrews, A., and Worthy, D.: Global CO_2 fluxes estimated from GOSAT retrievals of total column CO_2, Atmos. Chem. Phys., 13, 8695–8717, doi:10.5194/acp-13-8695-2013, 2013.

Basu, S., Krol, M., Butz, A., Clerbaux, C., Sawa, Y., Machida, T., Matsueda, H., Frankenberg, C., Hasekamp, O. P., and Aben, I.: The seasonal variation of the CO_2 flux over Tropical Asia estimated from GOSAT, CONTRAIL, and IASI, Geophys. Res. Lett., 41, 1809–1815, doi:10.1002/2013GL059105, 2014.

Chevallier, F., Engelen, R. J., and Peylin, P.: The contribution of AIRS data to the estimation of CO_2 sources and sinks, Geophys. Res. Lett., 32, doi:10.1029/2005GL024229, l23801, 2005.

Chevallier, F., Bron, F.-M., and Rayner, P. J.: Contribution of the Orbiting Carbon Observatory to the estimation of CO_2 sources and sinks: Theoretical study in a variational data assimilation framework, J. Geophys. Res.-Atmos., 112, doi:10.1029/2006JD007375, d09307, 2007.

Chevallier, F., Palmer, P. I., Feng, L., Boesch, H., O'Dell, C. W., and Bousquet, P.: Toward robust and consistent regional CO_2 flux estimates from in situ and spaceborne measurements of atmospheric CO_2, Geophys. Res. Lett., 41, 1065–1070, doi:10.1002/2013GL058772, 2013GL058772, 2014.

Crisp, D., Atlas, R., Breon, F.-M., Brown, L., Burrows, J., Ciais, P., Connor, B., Doney, S., Fung, I., Jacob, D., Miller, C., O'Brien, D., Pawson, S., Randerson, J., Rayner, P., Salawitch, R., Sander, S., Sen, B., Stephens, G., Tans, P., Toon, G., Wennberg, P., Wofsy, S., Yung, Y., Kuang, Z., Chudasama, B., Sprague, G., Weiss, B., Pollock, R., Kenyon, D., and Schroll, S.: The Orbiting Carbon Observatory (OCO) mission, Adv. Space Res., 34, 700 – 709, doi:10.1016/j.asr.2003.08.062, 2004.

Crisp, D., Pollock, H. R., Rosenberg, R., Chapsky, L., Lee, R. A. M., Oyafuso, F. A., Frankenberg, C., O'Dell, C. W., Bruegge, C. J., Doran, G. B., Eldering, A., Fisher, B. M., Fu, D., Gunson, M. R., Mandrake, L., Osterman, G. B., Schwandner, F. M., Sun, K., Taylor, T. E., Wennberg, P. O., and Wunch, D.: The on-orbit performance of the Orbiting Carbon Observatory-2 (OCO-2) instrument and its radiometrically calibrated products, Atmos. Meas. Tech., 10, 59–81, doi:10.5194/amt-10-59-2017, 2017.

Deng, F., Jones, D. B. A., Henze, D. K., Bousserez, N., Bowman, K. W., Fisher, J. B., Nassar, R., O'Dell, C., Wunch, D., Wennberg, P. O., Kort, E. A., Wofsy, S. C., Blumenstock, T., Deutscher, N. M., Griffith, D. W. T., Hase, F., Heikkinen, P., Sherlock, V., Strong, K., Sussmann, R., and Warneke, T.: Inferring regional sources and sinks of atmospheric CO_2 from GOSAT XCO_2 data, Atmos. Chem. Phys., 14, 3703–3727, doi:10.5194/acp-14-3703-2014, 2014.

Eldering, A., Boland, S., Solish, B., Crisp, D., Kahn, P., and Gunson, M.: High precision atmospheric CO_2 measurements from space: The design and implementation of OCO-2, in: 2012 IEEE Aerospace Conference, pp. 1–10, doi:10.1109/AERO.2012.6187176, 2012.

Eldering, A., O'Dell, C. W., Wennberg, P. O., Crisp, D., Gunson, M. R., Viatte, C., Avis, C., Braverman, A., Castano, R., Chang, A., Chapsky, L., Cheng, C., Connor, B., Dang, L., Doran, G., Fisher, B., Frankenberg, C., Fu, D., Granat, R., Hobbs, J., Lee, R. A. M., Mandrake, L., McDuffie, J., Miller, C. E., Myers, V., Natraj, V., O'Brien, D., Osterman, G. B., Oyafuso, F., Payne, V. H., Pollock, H. R., Polonsky, I., Roehl, C. M., Rosenberg, R., Schwandner, F., Smyth, M., Tang, V., Taylor, T. E., To, C., Wunch, D., and Yoshimizu, J.: The Orbiting Carbon Observatory-2: first 18 months of science data products, Atmos. Meas. Tech., 10, 549–563, doi:10.5194/amt-10-549-2017, 2017.

European Commission, Joint Research Centre (JRC)/Netherlands Environmental Assessment Agency (PBL): Emission Database for Global Atmospheric Research (EDGAR), release EDGARv4.2 FT2010, http://edgar.jrc.ec.europa.eu (last access: 15 Sep 2017), 2013.

Fang, Y. and Michalak, A. M.: Atmospheric observations inform CO_2 flux responses to enviroclimatic drivers, Global Biogeochem. Cy., 29, 555–566, doi:10.1002/2014GB005034, 2014GB005034, 2015.

Fang, Y., Michalak, A. M., Shiga, Y. P., and Yadav, V.: Using atmospheric observations to evaluate the spatiotemporal variability of CO_2 fluxes simulated by terrestrial biospheric models, Biogeosciences, 11, 6985–6997, doi:10.5194/bg-11-6985-2014, 2014.

Fischer, M. L., Parazoo, N., Brophy, K., Cui, X., Jeong, S., Liu, J., Keeling, R., Taylor, T. E., Gurney, K., Oda, T., and Graven, H.: Simulating estimation of California fossil fuel and biosphere carbon dioxide exchanges combining in situ tower and satellite column observations, J. Geophys. Res.-Atmos., 122, 3653–3671, doi:10.1002/2016JD025617, 2016JD025617, 2017.

Fisher, J. B., Sikka, M., Huntzinger, D. N., Schwalm, C., and Liu, J.: Technical note: 3-hourly temporal downscaling of monthly global terrestrial biosphere model net ecosystem exchange, Biogeosciences, 13, 4271–4277, doi:10.5194/bg-13-4271-2016, 2016.

Schaefer, K., Jacobso, A.R., Arain, M.A., Ciais, P., El-Masri, B., Hayes, D.J., Huang, M., Huang, S., Ito, A., Jain, A.K., Lei, H, Lu, C., Maignan, F., Mao, J., Parazoo, N.C., Peng, C., Peng, S. and Zhu, Q.: CMS: Modeled Net Ecosystem Exchange at 3-hourly Time Steps, 2004-2010. ORNL Distributed Active Archive Center, doi:10.3334/ornldaac/1315, 2016.

Giglio, L., Randerson, J. T., and van der Werf, G. R.: Analysis of daily, monthly, and annual burned area using the fourth-generation global fire emissions database (GFED4), J. Geophys. Res.-Biogeo., 118, 317–328, doi:10.1002/jgrg.20042, 2013.

Gourdji, S. M., Mueller, K. L., Schaefer, K., and Michalak, A. M.: Global monthly averaged CO_2 fluxes recovered using a geostatistical inverse modeling approach: 2. Results including auxiliary environmental data, J. Geophys. Res.-Atmos., 113, doi:10.1029/2007JD009733, d21115, 2008.

Gourdji, S. M., Mueller, K. L., Yadav, V., Huntzinger, D. N., Andrews, A. E., Trudeau, M., Petron, G., Nehrkorn, T., Eluszkiewicz, J., Henderson, J., Wen, D., Lin, J., Fischer, M., Sweeney, C., and Michalak, A. M.: North American CO_2 exchange: inter-comparison of modeled estimates with results from a fine-scale atmospheric inversion, Biogeosciences, 9, 457–475, doi:10.5194/bg-9-457-2012, 2012.

Griffith, D. A.: Effective geographic sample size in the presence of spatial autocorrelation, Ann. Assoc. Am. Geogr., 95, 740–760, doi:10.1111/j.1467-8306.2005.00484.x, 2005.

Guerlet, S., Basu, S., Butz, A., Krol, M., Hahne, P., Houweling, S., Hasekamp, O. P., and Aben, I.: Reduced carbon uptake during the 2010 Northern Hemisphere summer from GOSAT, Geophys. Res. Lett., 40, 2378–2383, doi:10.1002/grl.50402, 2013.

Gurney, K. R., Law, R. M., Denning, A. S., Rayner, P. J., Baker, D., Bousquet, P., Bruhwiler, L., Chen, Y.-H., Ciais, P., Fan, S., et al.: Towards robust regional estimates of CO_2 sources and sinks using atmospheric transport models, Nature, 415, 626–630, doi:10.1038/415626a, 2002.

Gurney, K. R., Mendoza, D. L., Zhou, Y., Fischer, M. L., Miller, C. C., Geethakumar, S., and de la Rue du Can, S.: High resolution fossil fuel combustion CO_2 emission fluxes for the United States, Environ. Sci. Technol., 43, 5535–5541, doi:10.1021/es900806c, pMID: 19708393, 2009.

Hammerling, D. M., Michalak, A. M., and Kawa, S. R.: Mapping of CO_2 at high spatiotemporal resolution using satellite observations: Global distributions from OCO-2, J. Geophys. Res.-Atmos., 117, doi:10.1029/2011JD017015, d06306, 2012.

Hammerling, D. M., Kawa, S. R., Schaefer, K., Doney, S., and Michalak, A. M.: Detectability of CO_2 flux signals by a space-based lidar mission, J. Geophys. Res.-Atmos., 120, 1794–1807, doi:10.1002/2014JD022483, 2014JD022483, 2015.

Heymann, J., Reuter, M., Buchwitz, M., Schneising, O., Bovensmann, H., Burrows, J. P., Massart, S., Kaiser, J. W., and Crisp, D.: CO_2 emission of Indonesian fires in 2015 estimated from satellite-derived atmospheric CO_2 concentrations, Geophys. Res. Lett., 44, 1537–1544, doi:10.1002/2016GL072042, 2016GL072042, 2017.

Houweling, S., Baker, D., Basu, S., Boesch, H., Butz, A., Chevallier, F., Deng, F., Dlugokencky, E. J., Feng, L., Ganshin, A., Hasekamp, O., Jones, D., Maksyutov, S., Marshall, J., Oda, T., O'Dell, C. W., Oshchepkov, S., Palmer, P. I., Peylin, P., Poussi, Z., Reum, F., Takagi, H., Yoshida, Y., and Zhuravlev, R.: An intercomparison of inverse models for estimating sources and sinks of CO_2 using GOSAT measurements, J. Geophys. Res.-Atmos., 120, 5253–5266, doi:10.1002/2014JD022962, 2014JD022962, 2015.

Huete, A., Didan, K., Miura, T., Rodriguez, E., Gao, X., and Ferreira, L.: Overview of the radiometric and biophysical performance of the MODIS vegetation indices, Remote Sens. Environ., 83, 195 – 213, doi:10.1016/S0034-4257(02)00096-2, 2002.

Huntzinger, D. N., Schwalm, C., Michalak, A. M., Schaefer, K., King, A. W., Wei, Y., Jacobson, A., Liu, S., Cook, R. B., Post, W. M., Berthier, G., Hayes, D., Huang, M., Ito, A., Lei, H., Lu, C., Mao, J., Peng, C. H., Peng, S., Poulter, B., Riccuito, D., Shi, X., Tian, H., Wang, W., Zeng, N., Zhao, F., and Zhu, Q.: The North American Carbon Program Multi-Scale Synthesis and Terrestrial Model Intercomparison Project – Part 1: Overview and experimental design, Geosci. Model Dev., 6, 2121–2133, doi:10.5194/gmd-6-2121-2013, 2013.

Japan Aerospace Exploration Agency: GOSAT-2: Greenhouse gas Observing SATellite-2, http://global.jaxa.jp/activity/pr/brochure/files/sat38.pdf (last access: 10 July 2017), 2017.

Joiner, J., Guanter, L., Lindstrot, R., Voigt, M., Vasilkov, A. P., Middleton, E. M., Huemmrich, K. F., Yoshida, Y., and Frankenberg, C.: Global monitoring of terrestrial chlorophyll fluorescence from moderate-spectral-resolution near-infrared satellite measurements: methodology, simulations, and application to GOME-2, Atmos. Meas. Tech., 6, 2803–2823, doi:10.5194/amt-6-2803-2013, 2013.

Jones, R. H.: Bayesian information criterion for longitudinal and clustered data, Stat. Med., 30, 3050–3056, doi:10.1002/sim.4323, 2011.

Kawa, S. R., Erickson, D. J., Pawson, S., and Zhu, Z.: Global CO_2 transport simulations using meteorological data from the NASA data assimilation system, J. Geophys. Res.-Atmos., 109, doi:10.1029/2004JD004554, d18312, 2004.

Law, R. M., Peters, W., Rödenbeck, C., Aulagnier, C., Baker, I., Bergmann, D. J., Bousquet, P., Brandt, J., Bruhwiler, L., Cameron-Smith, P. J., Christensen, J. H., Delage, F., Denning, A. S., Fan, S., Geels, C., Houweling, S., Imasu, R., Karstens, U., Kawa, S. R., Kleist, J., Krol, M. C., Lin, S.-J., Lokupitiya, R., Maki, T., Maksyutov, S., Niwa, Y., Onishi, R., Parazoo, N., Patra, P. K., Pieterse, G., Rivier, L., Satoh, M., Serrar, S., Taguchi, S., Takigawa, M., Vautard, R., Vermeulen, A. T., and Zhu, Z.: TransCom model simulations of hourly atmospheric CO_2: Experimental overview and diurnal cycle results for 2002, Global Biogeochem. Cy., 22, doi:10.1029/2007GB003050, gB3009, 2008.

Liu, J., Fung, I., Kalnay, E., and Kang, J.-S.: CO_2 transport uncertainties from the uncertainties in meteorological fields, Geophys. Res. Lett., 38, doi:10.1029/2011GL047213, l12808, 2011.

Maksyutov, S., Takagi, H., Valsala, V. K., Saito, M., Oda, T., Saeki, T., Belikov, D. A., Saito, R., Ito, A., Yoshida, Y., Morino, I., Uchino, O., Andres, R. J., and Yokota, T.: Regional CO_2 flux estimates for 2009–2010 based on GOSAT and ground-based CO_2 observations, Atmos. Chem. Phys., 13, 9351–9373, doi:10.5194/acp-13-9351-2013, 2013.

Miller, S. M., Hayek, M. N., Andrews, A. E., Fung, I., and Liu, J.: Biases in atmospheric CO_2 estimates from correlated meteorology modeling errors, Atmos. Chem. Phys., 15, 2903–2914, doi:10.5194/acp-15-2903-2015, 2015.

Mueller, K. L., Yadav, V., Curtis, P. S., Vogel, C., and Michalak, A. M.: Attributing the variability of eddy-covariance CO_2 flux measurements across temporal scales using geostatistical regression for a mixed northern hardwood forest, Global Biogeochem. Cy., 24, doi:10.1029/2009GB003642, gB3023, 2010.

NASA Jet Propulsion Laboratory: Orbiting Carbon Observatory 3, http://www.jpl.nasa.gov/missions/orbiting-carbon-observatory-3-oco-3/ (last access: 30 Aug 2017), 2017.

National Research Council: Verifying Greenhouse Gas Emissions: Methods to Support International Climate Agreements, The National Academies Press, Washington, DC, doi:10.17226/12883, 2010.

NOAA Global Monitoring Division: Global Greenhouse Gas Reference Network, https://www.esrl.noaa.gov/gmd/ccgg/ggrn.php (last access: 24 Aug 2017), 2017.

Olivier, J., Janssens-Maenhout, G., Munteam, M., and Peters, J.: Trends in global CO_2 emissions; 2014 Report, PBL Netherlands Environmental Assessment Agency; European Commission, Joint Research Centre, Ispra, Italy, http://edgar.jrc.ec.europa.eu/news_docs/jrc-2014-trends-in-global-co2-emissions-2014-report-93171.pdf (last access: 30 Aug 2017), 2014.

Olson, D. M., Dinerstein, E., Wikramanayake, E. D., Burgess, N. D., Powell, G. V. N., Underwood, E. C., D'amico, J. A., Itoua, I., Strand, H. E., Morrison, J. C., Loucks, C. J., Allnutt, T. F., Ricketts, T. H., Kura, Y., Lamoreux, J. F., Wettengel, W. W., Hedao, P., and Kassem, K. R.: Terrestrial ecoregions of the world: A new map of life on Earth, 51, 933–938, doi:10.1641/0006-3568(2001)051[0933:TEOTWA]2.0.CO;2, 2001.

Parazoo, N. C., Bowman, K., Frankenberg, C., Lee, J.-E., Fisher, J. B., Worden, J., Jones, D. B. A., Berry, J., Collatz, G. J., Baker, I. T., Jung, M., Liu, J., Osterman, G., O'Dell, C., Sparks, A., Butz, A., Guerlet, S., Yoshida, Y., Chen, H., and Gerbig, C.: Interpreting seasonal changes in the carbon balance of southern Amazonia using measurements of XCO_2 and chlorophyll fluorescence from GOSAT, Geophys. Res. Lett., 40, 2829–2833, doi:10.1002/grl.50452, 2013.

Ramsey, F. and Schafer, D.: The Statistical Sleuth: A Course in Methods of Data Analysis, Cengage Learning, Boston, MA, 2012.

Rienecker, M. M., Suarez, M. J., Gelaro, R., Todling, R., Bacmeister, J., Liu, E., Bosilovich, M. G., Schubert, S. D., Takacs, L., Kim, G.-K., Bloom, S., Chen, J., Collins, D., Conaty, A., da Silva, A., Gu, W., Joiner, J., Koster, R. D., Lucchesi, R., Molod, A., Owens, T., Pawson, S., Pegion, P., Redder, C. R., Reichle, R., Robertson, F. R., Ruddick, A. G., Sienkiewicz, M., and Woollen, J.: MERRA: NASA's Modern-Era Retrospective Analysis for Research and Applications, J. Climate, 24, 3624–3648, doi:10.1175/JCLI-D-11-00015.1, 2011.

Saeki, T., Maksyutov, S., Saito, M., Valsala, V., Oda, T., Andres, R. J., Belikov, D., Tans, P., Dlugokencky, E., Yoshida, Y., Morino, I., Uchino, O., and Yokota, T.: Inverse modeling of CO_2 fluxes using GOSAT data and multi-year ground-based observations, SOLA, 9, 45–50, doi:10.2151/sola.2013-011, 2013.

Schuh, A. E., Denning, A. S., Corbin, K. D., Baker, I. T., Uliasz, M., Parazoo, N., Andrews, A. E., and Worthy, D. E. J.: A regional high-resolution carbon flux inversion of North America for 2004, Biogeosciences, 7, 1625–1644, doi:10.5194/bg-7-1625-2010, 2010.

Schwarz, G.: Estimating the dimension of a model, Ann. Stat., 6, 461–464, http://www.jstor.org/stable/2958889, 1978.

Shiga, Y. P., Michalak, A. M., Randolph Kawa, S., and Engelen, R. J.: In-situ CO_2 monitoring network evaluation and design: A criterion based on atmospheric CO_2 variability, J. Geophys. Res.-Atmos., 118, 2007–2018, doi:10.1002/jgrd.50168, 2013.

Shiga, Y. P., Michalak, A. M., Gourdji, S. M., Mueller, K. L., and Yadav, V.: Detecting fossil fuel emissions patterns from subcontinental regions using North American in situ CO_2 measurements, Geophys. Res. Lett., 41, 4381–4388, doi:10.1002/2014GL059684, 2014GL059684, 2014.

Takagi, H., Saeki, T., Oda, T., Saito, M., Valsala, V., Belikov, D., Saito, R., Yoshida, Y., Morino, I., Uchino, O., Andres, R. J., Yokota, T., and Maksyutov, S.: On the benefit of GOSAT observations to the estimation of regional CO_2 fluxes, SOLA, 7, 161–164, doi:10.2151/sola.2011-041, 2011.

Takahashi, T., Sutherland, S., and Kozyr, A.: Global Ocean Surface Water Partial Pressure of CO_2 Database: Measurements Performed During 1957-2015 (Version 2015)., ORNL/CDIAC-160, NDP-088(V2015), Oak Ridge National Laboratory, U.S. Department of Energy, Oak Ridge, Tennesee, doi:10.3334/CDIAC/OTG.NDP088(V2015), 2016.

van der Werf, G. R., Randerson, J. T., Giglio, L., Collatz, G. J., Mu, M., Kasibhatla, P. S., Morton, D. C., DeFries, R. S., Jin, Y., and van Leeuwen, T. T.: Global fire emissions and the contribution of deforestation, savanna, forest, agricultural, and peat fires (1997–2009), Atmos. Chem. Phys., 10, 11 707–11 735, doi:10.5194/acp-10-11707-2010, 2010.

Wunch, D., Wennberg, P. O., Toon, G. C., Connor, B. J., Fisher, B., Osterman, G. B., Frankenberg, C., Mandrake, L., O'Dell, C., Ahonen, P., Biraud, S. C., Castano, R., Cressie, N., Crisp, D., Deutscher, N. M., Eldering, A., Fisher, M. L., Griffith, D. W. T., Gunson, M., Heikkinen, P., Keppel-Aleks, G., Kyrö, E., Lindenmaier, R., Macatangay, R., Mendonca, J., Messerschmidt, J., Miller, C. E., Morino, I., Notholt, J., Oyafuso, F. A., Rettinger, M., Robinson, J., Roehl, C. M., Salawitch, R. J., Sherlock, V., Strong, K., Sussmann, R., Tanaka, T., Thompson, D. R., Uchino, O., Warneke, T., and Wofsy, S. C.: A method for evaluating bias in global measurements of CO_2 total columns from space, Atmos. Chem. Phys., 11, 12 317–12 337, doi:10.5194/acp-11-12317-2011, 2011.

Wunch, D., Wennberg, P. O., Osterman, G., Fisher, B., Naylor, B., Roehl, C. M., O'Dell, C., Mandrake, L., Viatte, C., Kiel, M., Griffith, D. W. T., Deutscher, N. M., Velazco, V. A., Notholt, J., Warneke, T., Petri, C., De Maziere, M., Sha, M. K., Sussmann, R., Rettinger, M., Pollard, D., Robinson, J., Morino, I., Uchino, O., Hase, F., Blumenstock, T., Feist, D. G., Arnold, S. G., Strong, K., Mendonca, J., Kivi, R., Heikkinen, P., Iraci, L., Podolske, J., Hillyard, P. W., Kawakami, S., Dubey, M. K., Parker, H. A., Sepulveda, E., García, O. E., Te, Y., Jeseck, P., Gunson, M. R., Crisp, D., and Eldering, A.: Comparisons of the Orbiting Carbon Observatory-2 (OCO-2) $X_{\mathrm{CO_2}}$ measurements with TCCON, Atmos. Meas. Tech., 10, 2209–2238, doi:10.5194/amt-10-2209-2017, 2017.

Yokota, T., Yoshida, Y., Eguchi, N., Ota, Y., Tanaka, T., Watanabe, H., and Maksyutov, S.: Global Concentrations of CO_2 and CH_4 Retrieved from GOSAT: First Preliminary Results, SOLA, 5, 160–163, doi:10.2151/sola.2009-041, 2009.

Zucchini, W.: An Introduction to Model Selection, J. Math. Psychol., 44, 41 – 61, doi:10.1006/jmps.1999.1276, 2000.

Atmos. Chem. Phys. Discuss., https://doi.org/10.5194/acp-2017-813
Manuscript under review for journal Atmos. Chem. Phys.
Discussion started: 18 September 2017

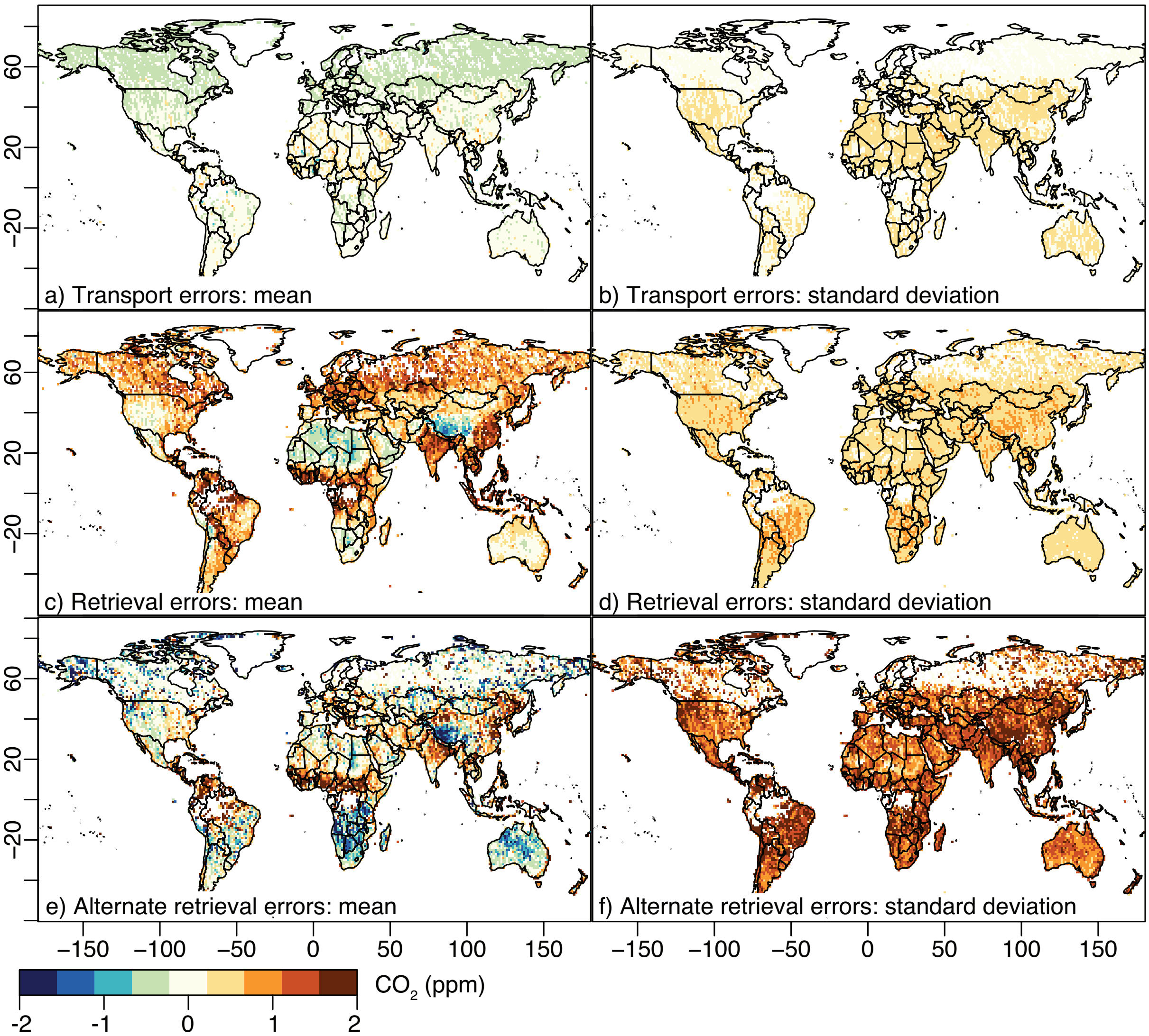

Figure 1. This figure displays the simulated synthetic data errors (i.e., simulated ϵ): the simulated atmospheric transport errors (a-b), the simulated observation/retrieval errors (c-d), and a second, alternative set of observation/retrieval errors (e-f). The left-hand panels display the mean of the errors within each PCTM grid box across the entire 2014–2015 study period, an indication of the correlation or covariance among the errors. By contrast, the right-hand panels display the standard deviation of the errors or residuals within each PCTM grid box.

Atmos. Chem. Phys. Discuss., https://doi.org/10.5194/acp-2017-813
Manuscript under review for journal Atmos. Chem. Phys.
Discussion started: 18 September 2017

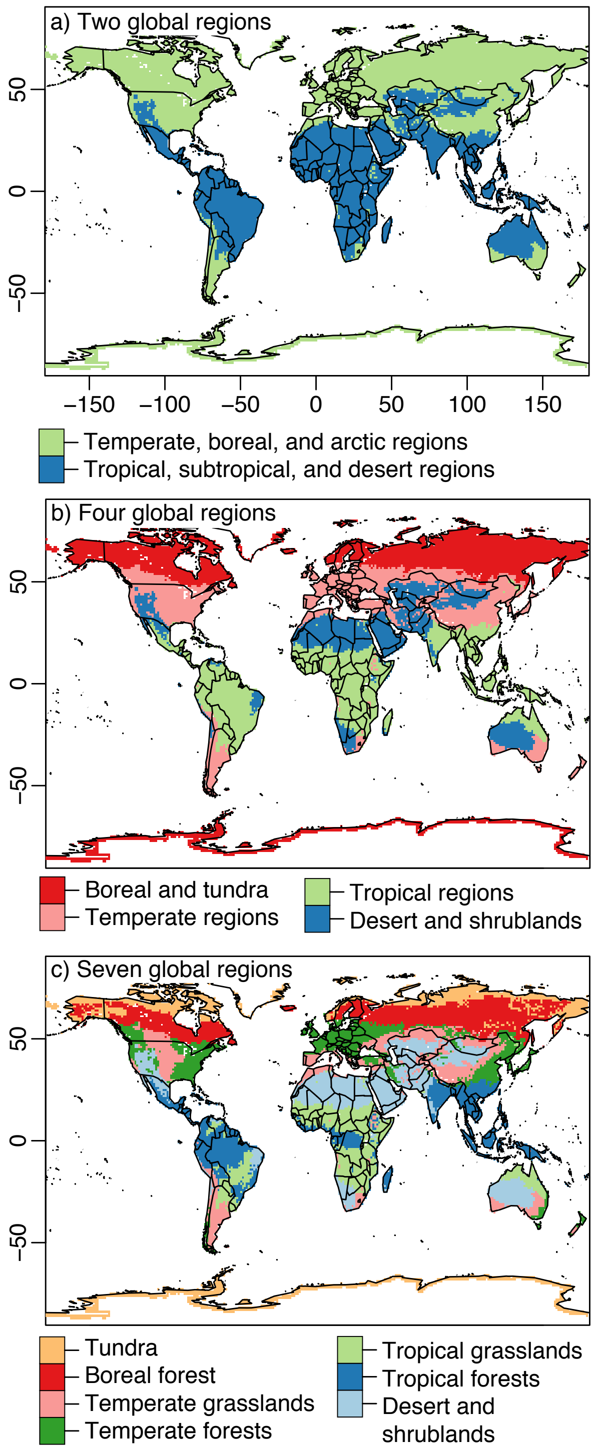

Figure 2. The two hemispheric regions (a), four continental regions (b), and seven biomes (c) used in this study. The biomes are based on a world biome map by Olson et al. (2001). The two and four region maps are amalgamated versions of the biomes.

Atmos. Chem. Phys. Discuss., https://doi.org/10.5194/acp-2017-813
Manuscript under review for journal Atmos. Chem. Phys.
Discussion started: 18 September 2017

Atmospheric Chemistry and Physics
Discussions

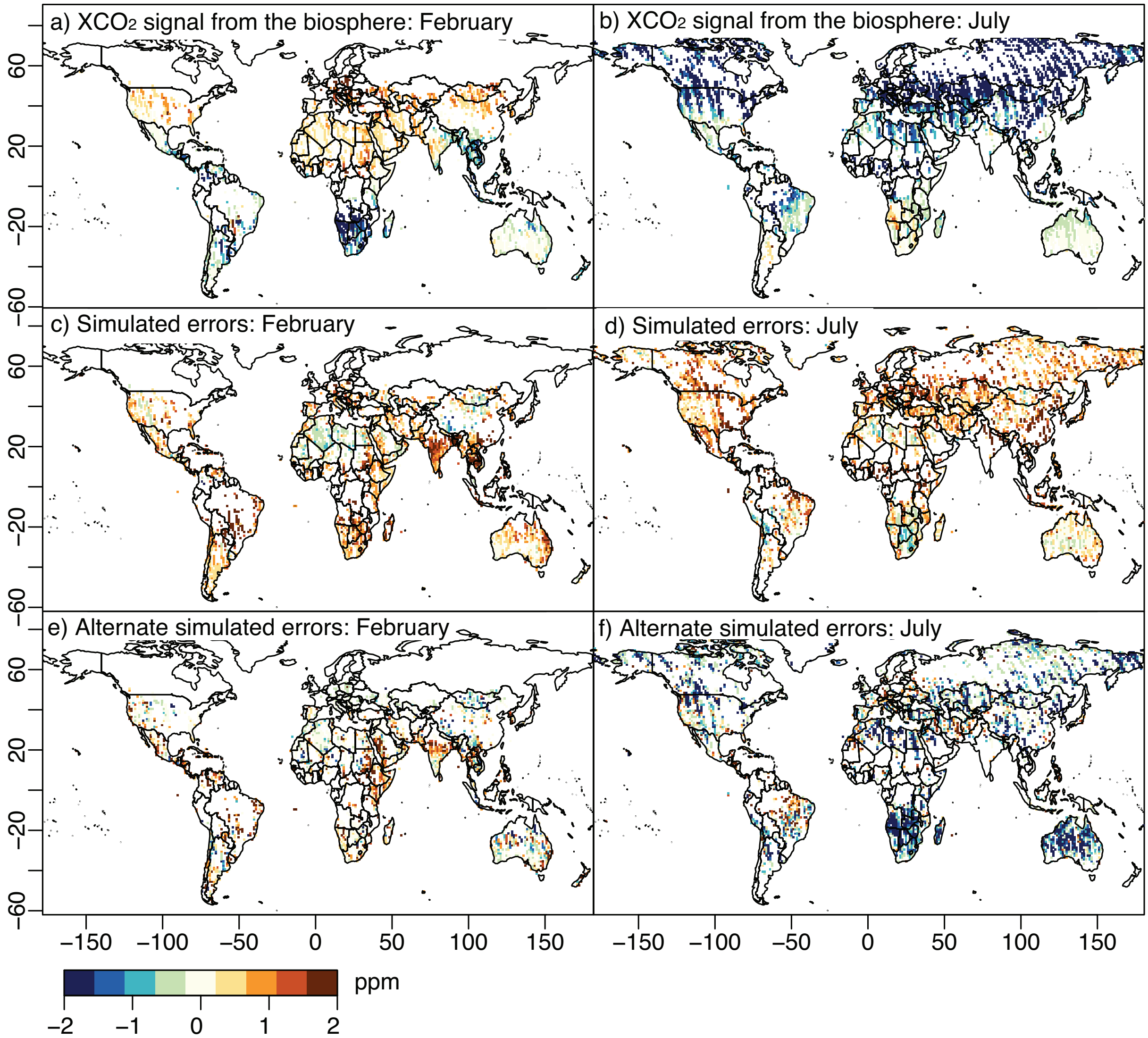

Figure 3. This figure compares the total column CO_2 or XCO_2 signal from biospheric fluxes against simulated model and observation errors. Panels a and b display the XCO_2 signal from biospheric CO_2 fluxes for February and July, respectively. We estimate this signal using the SiBCASA flux model and PCTM. Also note that the XCO_2 signal for February and July includes CO_2 fluxes from the months of February and July, respectively, and no fluxes from previous or subsequent months. Panels c and d represent the sum of both simulated observation and atmospheric transport errors (Sect. 2.1). Panels e and f show the sum of these errors using an alternate estimate for the retrieval errors.

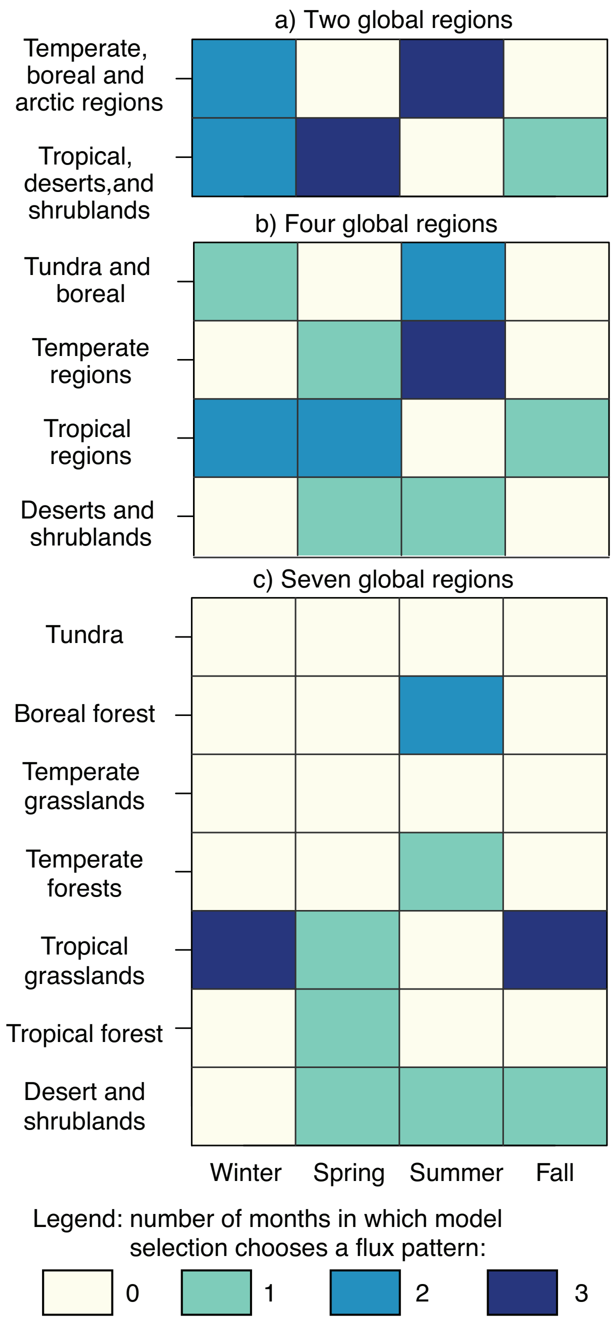

Figure 4. The results of the model selection experiments using real data. We select flux patterns for a greater fraction of regions/months in the two region case (a) than in the four or seven region cases (b and c). The different colors indicate the number of months in which model selection chooses a flux pattern for a given region.

Atmos. Chem. Phys. Discuss., https://doi.org/10.5194/acp-2017-813
Manuscript under review for journal Atmos. Chem. Phys.
Discussion started: 18 September 2017

Atmospheric Chemistry and Physics Discussions

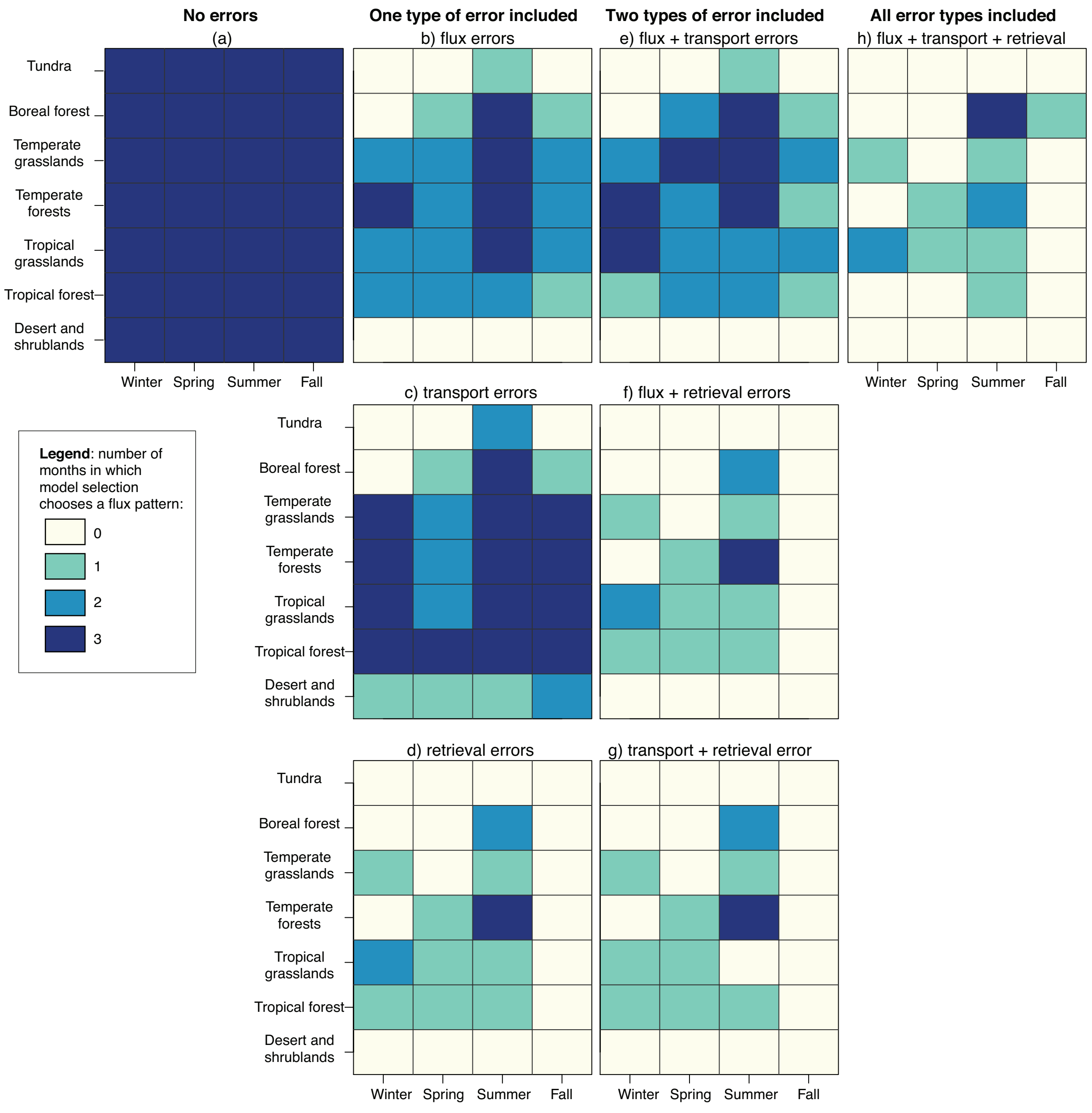

Figure 5. Model selection results for the synthetic data experiments. The first column (a) shows an experiment with no errors in the synthetic observations. The results of that experiment are ideal, and we choose a flux pattern in every month and every region using model selection. Subsequent panels (b-h) show the results with one, two, and three types of errors included. Fewer regions and seasons are selected in these experiments. The plot signals that observation or retrieval errors likely play a key role.